A new noncovalent force: Comparison of P···N interaction with hydrogen and halogen bonds

Steve Scheiner

Citation: The Journal of Chemical Physics **134**, 094315 (2011); doi: 10.1063/1.3562209
View online: http://dx.doi.org/10.1063/1.3562209
View Table of Contents: http://scitation.aip.org/content/aip/journal/jcp/134/9?ver=pdfcov
Published by the AIP Publishing

A new noncovalent force: Comparison of P · · · N interaction with hydrogen and halogen bonds

Steve Scheiner[a)]
Department of Chemistry and Biochemistry, Utah State University, Logan, Utah 84322-0300, USA

(Received 4 January 2011; accepted 14 February 2011; published online 7 March 2011)

When PH_3 is paired with NH_3, the two molecules are oriented such that the P and N atoms face one another directly, without the intermediacy of a H atom. Quantum calculations indicate that this attraction is due in part to the transfer of electron density from the lone pair of the N atom to the σ^* antibond of a P–H covalent bond. Unlike a H-bond, the pertinent hydrogen is oriented about 180° away from, instead of toward, the N, and the N lone pair overlaps with the lobe of the P–H σ^* orbital that is closest to the P. In contrast to halogen bonds, there is no requirement of a σ-hole of positive electrostatic potential on the P atom, nor is it necessary for the two interacting atoms to be of differing potential. In fact, the two atoms can be identical, as the global minimum of the PH_3 homodimer has the same structure, characterized by a P · · · P attraction. Natural bond orbital analysis, energy decomposition, and visualization of total electron density shifts reveal other similarities and differences between the three sorts of molecular interaction. © *2011 American Institute of Physics*. [doi:10.1063/1.3562209]

I. INTRODUCTION

The topic of noncovalent or intermolecular forces has motivated a great deal of work over the years, including a number of full monographs.[1–6] One of the most thoroughly researched areas has involved hydrogen bonds, due in part to the important role of this interaction in all sorts of processes from solvation to biomolecular structure and function. Despite the extensive research on H-bonds that goes back more than a century,[7–15] and which continues largely unabated, our understanding of this interaction continues to evolve. For example, recent research[16–23] has shown that the proton donor can be an atom such as C, less electronegative than the traditional O and N donors. The nature of the proton acceptor has been extended[24–31] beyond simple lone pairs to π bonds, σ bonds, metal atoms, and even another H atom. Indeed, the continuing widening of the definition of a H-bond has motivated a International Union of Pure and Applied Chemists (IUPAC) study group[32,33] to propose a new and more inclusive definition.

Other sorts of noncovalent interactions that have emerged from studies now include halogen bonds[34–39] which were perhaps initially surprising in that they involve the direct interaction between one electronegative atom and another. A prevailing picture as to how a nominally repulsive force such as this can actually be attractive arises with the idea that the electrostatic potential around the halogen atom is not wholly negative, but contains a small positive region, which can attract the electronegative partner atom. There are other cases in the literature of attractive forces between non-halogen electronegative atoms, such as S and O,[40–46] although they are not as well understood.

Along that vein, a recent set of calculations[47] that originally focused on the SH · · · N/P H-bonding capability of HSN noticed a second attractive force, between the N of HSN and the P atom of a phosphine. What was surprising about this interaction was first its strength, which appeared to be comparable to the traditional SH · · · N H-bond. More curious, however, was the fact that the P and N atoms were attracted to one another, without the presence of an intervening H atom as would be the case in a H-bond. Indeed, the $-PH_2$ group rotated itself in such a way as to avoid placing a H atom between the P and N, eschewing any possible H-bond. This behavior stood in marked contrast to the analogous amine, where the corresponding $-NH_2$ group did in fact orient itself so as to enable a NH · · · N H-bond.

The present work is dedicated to a more comprehensive examination of the attractive force between P and N atoms. Small molecules like PH_3 and NH_3 are used for this purpose so as to avoid any secondary interactions such as the SH · · · N H-bond that complicated the analysis in the earlier work. These small molecules also facilitate a thorough examination of the potential energy surfaces and a comprehensive analysis of the nature of the interaction, which is carried out via a number of complementary approaches, that address both individual molecular orbitals and total density shifts, as well as decomposition of the interaction energy by several different methods. A detailed comparison with both H-bonds and halogen bonds verifies that the P · · · N interaction does indeed represent a new sort of noncovalent intermolecular force.

II. COMPUTATIONAL METHODS

Calculations were carried out using the GAUSSIAN 03 package.[48] All geometries were optimized at the *ab initio* MP2 level, using the aug-cc-pVDZ basis set, designed specifically[49] for correlated calculations. Minima were identified using a range of starting points for geometry optimizations; structures were verified as minima by having all real vibrational frequencies. Interaction energies were computed

a)Electronic mail: steve.scheiner@usu.edu.

as the difference in energy between the dimer and the sum of the optimized energies of the isolated monomers. These quantities were corrected for basis set superposition error by the counterpoise procedure,[50] and by zero-point vibrational energies. Natural bond orbital (NBO) analysis[51,52] was carried out via the procedures contained within GAUSSIAN 03. The interaction energy was decomposed by two different schemes. The GAMESS-US version 2010 R1 program[53] was used to perform the Kitaura–Morokuma (KM) decomposition,[54,55] and the symmetry-adapted perturbation theory procedure[56,57] was implemented via the MOLPRO set of codes.[58] Density shifts were visualized and plotted via the MOLDEN program.[59]

III. RESULTS

A thorough search was conducted for minima on the surface of the PH_3/NH_3 heterodimer, using a number of different structures as starting points for optimization. Some of these candidate geometries included a cyclic H-bond wherein both NH and PH bonds are oriented toward the other molecule, with both H-bonds distorted from linearity. Trifurcated structures were also considered as starting points wherein all three PH bonds were oriented toward the N, and vice versa, which would best align the dipole moments of the two molecules.

The only two minima ultimately located on the heterodimer surface are illustrated in Fig. 1. The more stable of the two, **1a**, has the P and N atoms directly facing one another without the intermediacy of an intervening H atom. Instead, there are two H atoms that are set nearly 180° away from the P···N axis, at angles of 168° and 161° from this axis. The secondary minimum, **1b**, more nearly fits the classical description of a H-bond wherein the P–H bond lies within 7° of the P···N axis, making for the traditional connection between this bridging H atom and the N lone pair. The latter lone pair, defined by the C_3 axis of the NH_3 subunit, lies within 1° of this bridging H. The P and N atoms are separated by 4.049 Å in **1b**, considerably longer than the P···N distance of 3.302 Å in the global minimum.

The energetics of binding in the two minima are reported in Table I, from which it may be seen that **1a** is more stable than **1b** by about 0.5 kcal/mol before and after counterpoise and zero-point vibrational energy (ZPE) corrections. Indeed, with both of these corrections included **1b** becomes essentially equal in energy to the isolated PH_3 and NH_3 monomers, with zero binding energy. The next row of Table I reiterates the considerably longer P···N interatomic distance in **1b**.

The direct interaction between the P and N atoms is unexpected in certain respects so bears more detailed scrutiny. In the first place, one might anticipate that P and N, both lying

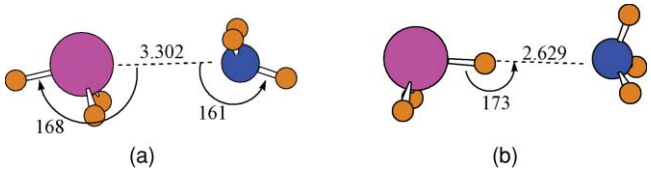

FIG. 1. Geometries of global (a) and secondary (b) minima of the heterodimer between PH_3 and NH_3. Angles in degrees and distances in Å.

TABLE I. Energetics (kcal/mol) and geometrical parameters of two minima in surface of $PH_3 + NH_3$ surface.

	1a	1b
ΔE	−2.05	−1.53
$\Delta E + CC$[a]	−1.43	−0.83
$\Delta E + CC + ZPE$[b]	−0.41	+0.04
R(P···N) (Å)	3.302	4.049
Δr(P/N–H)[c] (mÅ)	2.8, 0.4	0.7

[a]Counterpoise correction.
[b]Zero-point vibrational energy correction.
[c]Changes in P–H or N–H bonds that accept charge into σ^* antibond.

in the same column of the periodic table, should bear similar atomic charges. And indeed, the dipole moments of PH_3 and NH_3 are alike in the sense that both point in the same direction, with its negative pole along the direction of the P or N lone pair. On the other hand, there is a substantial difference in electronegativity between P and N, which accounts for the larger magnitude of the dipole moment of NH_3, more than twice that of PH_3.

The P and N atomic charges are quite different as well. Of course, there are numerous ways in which to evaluate these quantities, some provide more sensible values than others. First with respect to Mulliken charges, the P of isolated PH_3 is assigned a charge of −0.62 as compared to an atomic charge of −0.05 on N of NH_3. Given the greater electronegativity of N, this pair of values is counterintuitive, and underscores the arbitrary nature of Mulliken charges. Indeed, APT charges of +0.29 and −0.41 for P and N, respectively, are in better consonance with chemical intuition as are the NBO charges of +0.11 and −1.10. Given their opposite atomic charges, the direct approach of the P and N in **1a** becomes more sensible. Yet at the same time, the attraction is not purely electrostatic, as detailed below. (Recall that the charges on the H atoms in these molecules are simply −1/3 the value of q_P or q_N.)

A. Energy decompositions

Of course the P and N atomic charges only provide a hint of the magnitude of the electrostatic interaction, evaluation of which requires a more rigorous formulation. The Kitaura-Morokuma (KM) energy partitioning scheme is one such method which evaluates the electrostatic interaction between the electron distributions of the two monomers, prior to mutual polarizations or charge transfer. The quantities reported in the first row of Table II indicate that there is indeed a rather strong contribution of electrostatic (ES) attraction in **1a**. This quantity is a full kcal/mol greater than the electrostatic component of **1b**, which as a H-bonded complex, relies to a large extent on ES for its stability. The second row of Table II indicates greater exchange repulsion (EX) in **1a** than in **1b**, consistent with the closer proximity of the two monomers and the consequently greater degree of interpenetration of their electron clouds. The second-order energies, reflecting the adjustment of each monomer's density to perturbations caused by the presence of its partner, are reported in the next two rows of Table II. Polarization (POL) refers to redistributions within each monomer, and charge transfer (CT)

TABLE II. Kitaura–Morokuma partitioning of the interaction energy of the two configurations of the PH_3/NH_3 heterodimer. All quantities in kcal/mol.

	1a	1b
ES	−2.70	−1.73
EX	3.22	2.80
POL	−1.03	−0.48
CT	−0.74	−0.81
CORR[a]	−1.26	−0.87
MIX	+0.86	+0.24

[a]Correlation energy corrected for BSSE.

to those that take place from one molecule to the other. While **1a** and **1b** display very similar amounts of charge transfer, there is more than twice as much polarization stabilization in **1a** as in **1b**. The next row of Table II refers to the contribution made by electron correlation to the interaction energy. This quantity, CORR, was computed as the difference between the MP2 and SCF binding energies, with both corrected for basis set superposition error. CORR offers a rough approximation to dispersion energy, although it is not quite the same thing. In any case, it is clear that there is a greater correlation contribution to the binding energy in **1a** than in **1b**. The last row of Table II reports the so-called mixing (MIX) energy of the KM formulation which is not easily classified in any of the forgoing categories. In summary, in comparison to H-bonded structure **1b**, the **1a** configuration contains significantly greater ES and POL contributions as well as a larger correlation component.

Of course, the KM scheme is only one of the several means of partitioning the total interaction energy into physically meaningful components. A second procedure that is widely used is symmetry-adapted perturbation theory (SAPT). The two procedures have certain features in common, particularly at first order, but there are also significant differences.[60] The ES and EX components displayed in the first two rows of Table III are, not surprisingly, quite similar to those obtained by the KM approach. The induction energy (IND) describes second-order perturbations of the electron clouds, so is to some extent comparable to the sum of the KM POL + CT. And like the KM analysis, the SAPT IND energy is more attractive for **1a** than for **1b**. Induction also has an exchange component, which, when added in the next row of Table III as IND + EXIND, leaves a much less attractive contribution. This term is rather small for both minima, less than 0.5 kcal/mol. The dispersion energy (DISP) in the next row of Table III is fairly large, almost as attractive as the ES component, and is more prominent for **1a** than for **1b**. When the exchange part of the dispersion is added, the full dispersion energy in the last row of Table III is a bit less attractive, but retains the preference of **1a** over **1b**. In summary, KM and SAPT provide complementary data for the two minima, and agree on most of the major points.

TABLE III. SAPT partitioning of the interaction energy of the two configurations of the PH_3/NH_3 heterodimer. All quantities in kcal/mol.

	1a	1b
ES	−2.68	−1.71
EX	3.16	2.71
IND	−1.68	−0.87
IND + EXIND	−0.34	−0.47
DISP	−2.04	−1.51
DISP + EXDISP	−1.72	−1.26

TABLE IV. NBO charge transfer and second-order perturbation energies of the two configurations of the PH_3/NH_3 heterodimer.

	Δq^a (me)	Δq^b (me)	$E(2)$ (kcal/mol)
1a			
$P_{lp} \rightarrow \sigma^*NH$	0.4	0.6	0.32
$N_{lp} \rightarrow \sigma^*PH$	2.0	3.8	1.18
1b			
$N_{lp} \rightarrow \sigma^*PH$	4.6	5.1	2.82

[a]Computed as $2 \times (F_{ij}/\Delta\varepsilon)^2$.
[b]Occupation change of NBO σ^*.

Structure **1b** has all the hallmarks of a H-bond. The bridging H atom lies almost directly along the P · · · N axis, and the largest component of the interaction energy is ES, followed by CT and POL, augmented by a fairly large correlation contribution. There is also a small stretch of the bridging P–H covalent bond, in this case by 0.0007 Å.

B. Charge shifts

It is usually accepted that the latter covalent bond stretch in a H-bonded structure is caused primarily by a shift of electron density from the lone pair of the proton-accepting (N) atom to the P–H σ^* antibonding orbital. Indeed, NBO analysis bears out this idea. This quantity was calculated first according to the NBO formalism in terms of the Fock matrix element between the two orbitals F_{ij}, and their difference in energy, ε_{ij}. It was also computed simply as the difference in occupation of the P–H σ^* in the complex relative to the isolated monomer. As reported in the last row of Table IV, there is roughly a 5 me transfer of density in **1b**, computed by either means. The last row of Table IV also displays the NBO $E(2)$ quantity which is an energetic consequence of this charge transfer, and amounts to 2.8 kcal/mol.

Although **1a** does not have a bridging H atom between the P and N atoms, it does have a certain degree of resemblance to the H-bonded structure **1b**. NBO analysis reveals a charge transfer from the N lone pair to the P–H σ^* antibond. The overlap between these two orbitals occurs via the antibonding lobe that lies along the P–H direction, opposite the P–H hydrogen, as illustrated by the curved arrow in Fig. 2. There is a smaller, but still appreciable, transfer from the P lone pair to the corresponding N–H σ^* antibond. The energetic consequences of these two transfers, $E(2)$, are 1.18 and 0.32 kcal/mol, respectively, as reported in the last column of Table IV. Together these two transfers sum to 1.50 kcal/mol, roughly half than that in **1b**. The charge transfers that occur, computed in two different ways, are also smaller than those observed in H-bonded structure **1b**. Both of these charge transfers are facilitated by the nearly 180° angles

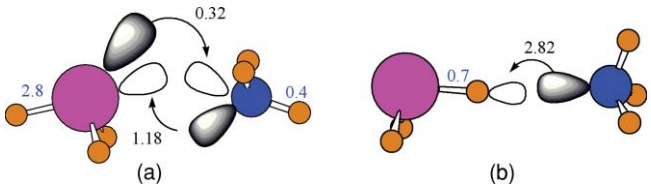

FIG. 2. NBO analyses of the PH_3/NH_3 heterodimer illustrating density transfer from lone pairs of P and N (filled lobe) to σ^* P–H/N–H antibonding orbitals (unfilled lobe). Values of $E(2)$ for each transfer are shown in kcal/mol in black. Blue numbers correspond to stretch of indicated P–H or N–H covalent bond caused by formation of complex, in mÅ.

between each of these P/N–H bonds and the N/P atom of its partner. The other evidence of density accumulation in the P–H σ^* antibond arises from the stretch of this covalent bond which may be seen to be 2.8 mÅ in Fig. 2. This quantity is considerably larger than the 0.4 mÅ stretch of the corresponding N–H bond, which is consonant with the smaller charge shift into the latter antibond. It is interesting that this stretch is also four times larger than that of the bridging P–H bond in **1b**, despite the smaller measures of charge shift in **1a**.

Another window into the fundamental nature of the interactions arises from monitoring the shifts of total electron density that accompany the formation of each dimer. These shifts are illustrated in Fig. 3 where the green areas represent increases of density, and decreases indicated by brown. Structure **1b** obeys the typical trends for H-bonded systems which include a large loss of density around the bridging H, and increases on the proton-acceptor (N) lone pair, and in the region between the H and the donating (P) atom. (It should be recalled that the patterns of total density shift in Fig. 3 are not expected to mirror the density shifts that occur within any one orbital or pair of orbitals, which are emphasized in the NBO formalism.) The pattern in **1a** also indicates a density increase in the N lone pair, but there are some important differences as well. Rather than a large brown decrease around the bridging H in **1b**, this loss occurs on the right side of the P atom, even if there is no atom present in that region. The green buildup of charge in the bridging P–H bond of **1b** is completely absent in **1a** and occurs instead in the H atom that is directly opposite the N.

C. Anisotropy

Given the presence of two minima in the surface of the heterodimer, the level of anisotropy of the interaction energy is of some interest. In other words, since the NH_3 is located

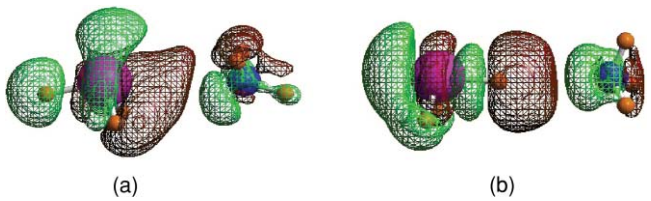

FIG. 3. Density shifts occurring in the PH_3/NH_3 heterodimer upon formation of each complex. Green regions indicate density increase, brown a decrease. Contours are shown at the 0.0002 a.u. level.

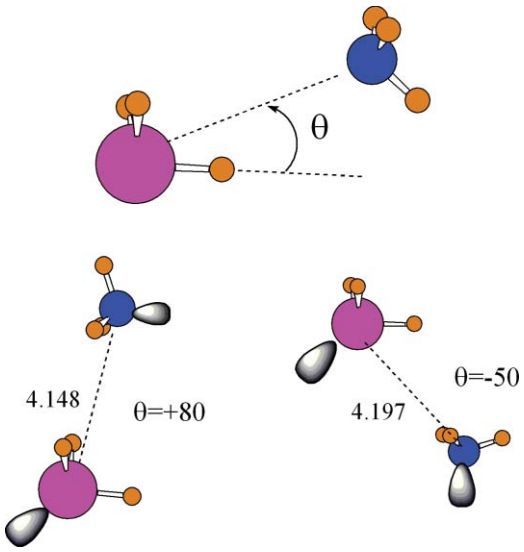

FIG. 4. Definition of angle θ which specifies position of NH_3 relative to P–H bond. Barriers to interconversion of the two minima occur at $\theta = +80^\circ$ and -50°, both of which are illustrated, along with lone pairs, defined as C_3 axis of each molecule.

along a P–H bond in **1b**, and almost completely opposite this position in **1a**, it is natural to wonder how the energy behaves at intermediate positions, and what sort of barrier is present to the interconversion of the two minima. The dispersion energy is typically less anisotropic than other contributions, e.g., electrostatics, so if the former were the dominant attractive force, one might anticipate a lower sensitivity of the energy as one or the other molecules is rotated around its partner.

In order to answer this question, the NH_3 was placed at a number of fixed angles θ, defined in Fig. 4, from a P–H bond of PH_3, and the geometry fully optimized with this single angular restraint. It was found that the two minima, **1a** and **1b**, are separated by a barrier that lies some 1.2 kcal/mol above the global minimum. This barrier occurs at θ angles of $+80^\circ$ and -50°, at which point the (counterpoise-corrected) interaction energy is only -0.2 kcal/mol. Even this small degree of binding is eliminated when ZPE is included. These structures are illustrated in the lower part of Fig. 4 where it may be seen first that both involve fairly long P · · · N distances, in excess of 4 Å, much longer than the 3.3 Å of **1a**. It is clear as well that in both of these high-energy geometries, neither the P nor the N lone pairs are favorably disposed to interact with the partner molecule. In the case of $\theta = +80^\circ$, the P lone pair is oriented nearly 180° from the N, while the angle between N atom and the P lone pair is close to 90° when $\theta = -50^\circ$. And the reader is reminded that the lone pair of each molecule is coincident with its dipole moment, for purposes of thinking about electrostatic forces.

D. PH_3 homodimer

The PH_3/NH_3 heterodimer can form a H-bonded complex as one of its minima in part because the lone pair of NH_3 is an excellent proton acceptor. But if both molecules are PH_3, which has a central atom with a partial positive charge, a H-bond becomes less tenable. And indeed, there is no H-bonded

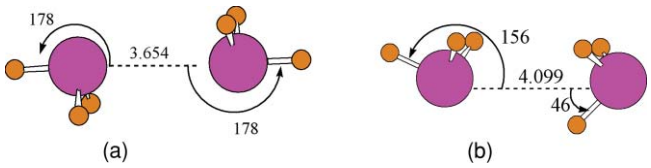

FIG. 5. Geometries of global (a) and secondary (b) minima of the PH_3 homodimer. Angles in degrees and distances in Å.

structure that corresponds to a minimum on the $(PH_3)_2$ surface. The two minima located are displayed in Fig. 5. Structure **5a** is a symmetrical geometry along the same lines as the heterodimer **1a**. The two P atoms directly approach one another, and each molecule has one P–H bond directly opposite the P · · · P axis. Other than a slightly more weakly bound homodimer, with a longer intermolecular separation, the energetics and geometries reported in Table V reinforce the similarities between **5a** and **1a**.

Structure **5b**, however, is quite unique and even anomalous in some ways. More weakly bound than **5a**, the lone pair of the right hand molecule is turned away from that on the left so it cannot donate electron density. There is perhaps a weak H-bond between the lone pair of the molecule on the left and one of the right hand P–H bonds, but with considerable misalignment, as is evident in Fig. 5. In any case, it is clear that electrostatic interactions alone cannot account for the stability of this structure.

SAPT analysis of these dimers in Table VI supports the fundamental similarity of **1a** and **5a**. There is a reduction of the ES and EX terms in **5a**, but the IND and DISP terms are both a little larger. Both of the latter increases might be expected based on the change from a first- to a second-row atom. The components of **5b** are quite different. This interaction is dominated by dispersion, which is more than twice as large as the electrostatic attraction, with only a small induction contribution, which is extinguished when EXIND is added. KM analysis supports the SAPT ideas, in that the correlation energy is quite similar to the SAPT dispersion energy, with similar values for ES and EX. Without the exchange effects, KM yields a combined POL + CT contribution that is nearly equal to the ES term, similar to the SAPT conclusion in Table VI.

The NBO analysis of **5a** supports the idea that P lone pair charge is transferred to the P–H σ^* antibond, analogously to **1a**. The $E(2)$ energy of each $P_{lp} \rightarrow \sigma^*PH$ transfer is equal to 1.04 kcal/mol, quite similar to the 1.18 kcal/mol for $N_{lp} \rightarrow \sigma^*PH$ transfer in **1a**. The two measures of charge transferred

TABLE V. Energetics (kcal/mol) and geometrical parameters of two minima in surface of PH_3 homodimer.

	5a	5b
ΔE	−1.72	−1.29
ΔE + CC[a]	−1.14	−0.74
ΔE + CC + ZPE[b]	−0.37	−0.15
R(P · · · P) (Å)	3.654	4.099
Δr(P–H)[c] (mÅ)	1.6	0.9

[a]Counterpoise correction.
[b]Zero-point vibrational energy correction.
[c]Changes in P–H bonds that accept charge into σ^* antibond.

TABLE VI. SAPT partitioning of the interaction energy of the two configurations of the PH_3 homodimer. All quantities in kcal/mol.

	5a	5b
ES	−1.83	−0.77
EX	2.98	1.89
IND	−2.07	−0.75
IND + EXIND	−0.22	−0.07
DISP	−2.26	−1.92
DISP + EXDISP	−1.94	−1.71

are also slightly larger than those for **1a**, so this facet of the interaction would appear to be rather strong in **5a**. This greater degree of charge transfer is also supported by the larger value of IND in **5a** as compared to **1a**. Also consistent with the pattern in **1a**, the P–H bond is elongated as density is moved into its σ^* antibond, albeit by not as much as in **1a**. In contrast, there is very little charge transfer in **5b** from the P lone pair to the P–H antibond that could conceivably act as electron acceptor, which argues against considering this geometry as H-bonded.

The density shifts in the PH_3 homodimer are illustrated in Fig. 6, wherein comparison of **5a** with **1a** in Fig. 3 reinforces their similarity. Both contain green regions of density gain in the areas of the P or N lone pairs as well as gain on the H atoms whose σ^* antibond accepts density. The shifts in **5b** are very small indeed, with no change apparent in the left hand molecule at the 0.0002 a.u. contour level. A region of loss surrounding the H atom on the right side is consistent with a very weak PH · · · P H-bond, although this idea is not confirmed by a gain of density in the lone pair region of the proton acceptor on the left.

E. Comparison with halogen bonds

The type of interaction described here, in which two nominally electronegative atoms, such as N and P, or P and P, approach one another directly without an intervening H, might put one in mind of halogen bonds, which have been extensively explored over the last few years.[61–64] However, there appear to be a number of fundamental distinctions between the two. One view[65–70] considers halogen bonds as primarily electrostatic, based upon a σ-hole of positive electrostatic potential that develops on the halogen atom, in contrast to its overall negative charge, which can facilitate an attraction with a negatively charged counterpart atom on the partner molecule. The P · · · N interaction described here differs first of all in that P contains a partial positive charge, not the

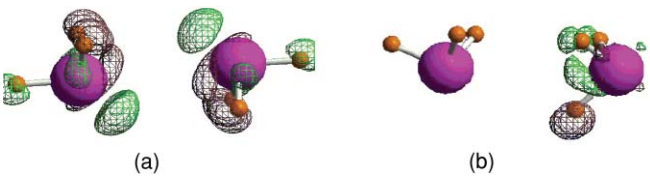

FIG. 6. Density shifts occurring in the PH_3 homodimer upon formation of each complex. Green regions indicate density increase, brown a decrease. Contours are shown at the 0.0002 a.u. level.

negative overall charge of the halogens. Nor is there found any indication of a σ-hole in the electrostatic potential of PH_3, a conclusion that is verified by prior study of a number of phosphines.[71] And even were such an anisotropic distribution of electrostatic potential present on P, the symmetric geometry of **5a** would yield a repulsive force anyway. So this picture of halogen bonding is not tenable for P···N and P···P.

Other workers attribute the primary attractive force of halogen bonding to induction[72,73] or to dispersion forces.[6,74] According to the data presented above for the P···N bond in Tables II and III, the Kitaura–Morokuma formulation might support some role for induction, as does SAPT (when exchange-induction is not included in the IND component). On the other hand, either the exchange-free SAPT induction, or the sum of the KM charge transfer and polarization energies, still comprise only a fraction of the ES component. Dispersion forces cannot be discounted, but here again, the SAPT DISP is smaller than ES, either with or without exchange-dispersion included. Both induction and dispersion become more important for the PH_3 homodimer, wherein their contributions are comparable to that of ES.

In order to more explicitly draw out this comparison, calculations were carried out for the halogen bond connecting CH_3Br with H_2CO, using the same level of theory applied here to the P···N and P···P complexes. The pair was chosen as previous calculations[6] suggest that its total binding energy is similar in scale to the PH_3/NH_3 heterodimer, so energy components should be directly comparable. Indeed, the binding energy computed here for $CH_3Br\cdots OCH_2$ is -1.27 kcal/mol after counterpoise correction, quite close to the value of -1.43 kcal/mol calculated for the same property in PH_3/NH_3. In comparison to the latter, the interaction energy of $CH_3Br\cdots OCH_2$ has a smaller SAPT electrostatic attraction but larger dispersion and induction components, along with a greater exchange repulsion. Within the KM scheme the halogen bond contains a larger charge transfer component, -1.06 versus -0.74 kcal/mol. Analogous to the P···N bond, the halogen bond displays a certain degree of NBO charge transfer from the O lone pairs to the C–Br σ^* antibond, comparable in magnitude to $E(2)$ for the $N_{lp} \rightarrow \sigma^*PH$ transfer, although the corresponding stretch of the C–Br bond is only 0.3 mÅ, an order of magnitude smaller than the P–H stretch for P···N.

The density redistribution pattern of the halogen bond, portrayed in Fig. 7, shows certain elements in common with the P···N interaction of Fig. 3(a). In both cases, there is a broad area of density loss by the P/Br electron acceptor atom, and a green gain area perpendicular to this region. However, unlike the P···N bond, where there is clear gain in the region of the N lone pair, no such increase is observed around the O atom of the Br···O bond. Whereas the leftmost H atom of Fig. 3(a), the recipient of density via the $N_{lp} \rightarrow \sigma^*$(P–H) transfer, is surrounded by a density gain in the P···N bond, the increase in the halogen-bonded system occurs instead right along the Br–C bonding region.

Another point of comparison between the P···N and halogen bonds is associated with the angular constraints. As noted by several research groups, the positively charged σ-hole on the halogen atom is ringed by the negative charge

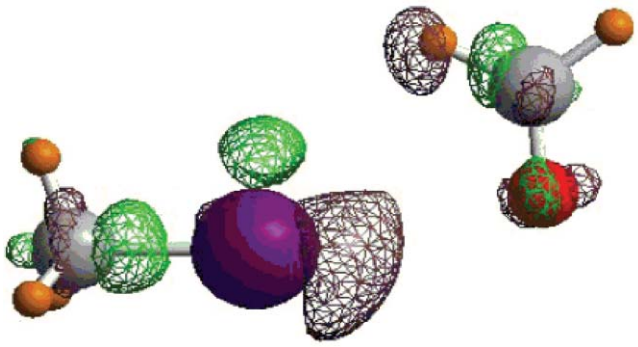

FIG. 7. Density shifts occurring in the halogen-bonded $CH_3Br\cdots OCH_2$ complex. Green regions indicate density increase, brown a decrease. Contours are shown at the 0.0002 a.u. level.

of the rest of this atom. This electrostatic potential anisotropy leads to a strong angular dependence of the halogen bond. For example, the θ(C–Br···O) angle in the optimized geometry of $CH_3Br\cdots OCH_2$ was found to be 169°, close to the 180° value expected for the maximal positive electrostatic potential in the Br atom. Attempts to assess the angular dependence of the interaction energy were unsuccessful because if θ is changed by even a little from its optimal value, to 150° or 130°, for example, this bonding is lost: the H_2CO molecule pivots around the O atom so as to bring one or both of its H atoms toward the Br, with a CH···Br H-bond replacing the halogen bond entirely. This behavior is fundamentally distinct from that of the PH_3/NH_3 heterodimer where the interaction is anisotropic to some degree, but there is no precipitous change from one sort of interaction to another.

A comprehensive summary and comparison of P···N, H-bonding, and halogen bonding can be gleaned by examination of Table VII. The first two columns pertain to the P···N interaction and its P···P cousin, followed by the H-bond of complex **1b**; the halogen bond contained in $CH_3Br\cdots OCH_2$ comprises the final column. The first row relates to the change of NBO atomic charge upon the N, P, or O atom that serves as electron donor in each case, and shows that each of these atoms becomes more negatively charged upon complexation, a point of similarity for all. The largest increase in this negative charge is associated with the P···N/P interactions of the first two columns. The next row illustrates the much more positive charge on the shared proton of the H-bond, twice as large as that observed in the bridging Br of the halogen bond. There is no bridging H or Br atom in the P···N/P bond, so Table VII instead reports the change in the comparable H atoms, that point away from the electron donor, acquiring density in the appropriate σ^* antibond. Note that these H atoms behave in an opposite fashion, becoming more negative in the case of the stronger interaction.

The next three rows of Table VII report the changes in occupation of several NBO orbitals that arise from the interaction. The increases expected in the P–H or C–Br σ^* antibonds are greatest for the H-bond, with the other three all showing a smaller increase of some 3 me. Concurrent with antibond population increase is a smaller diminution in the σ bonding orbital, reported in the next row. And all sorts of interactions share a drop in the occupation number of the lone pair of

TABLE VII. Changes in NBO atomic charges, occupation numbers, orbital energies resulting from complexation, and charge transfer energies measured in various ways.

	P · · · N 1a	P · · · P 5a	PH · · · N 1b HB	C–Br · · · O
q N/P/O (me)	−7.5	−8.2	−4.4	−5.8
q H/Br (me)	−11.9	0.3	+34.9	+18.5
Occ. P–H*/C–Br* (me)	3.8	3.1	5.1	2.8
Occ. P–H/C–Br (me)	−1.1	−0.9	−1.0	−0.4
Occ. N/P/O lp (me)	−4.1	−4.5	−5.1	−2.1/−0.7[a]
ε_{lp} (10^{-3} a.u.)	−3.8	+3.5	−6.4	4.1/4.6[a]
ε_{σ^*} (10^{-3} a.u.)	16.2	7.9	35.3	14.2
$\sum E(2)$ (kcal/mol)	1.50	2.08	2.82	1.09
SAPT IND (kcal/mol)	−1.68	−2.07	−0.87	−2.37
KM CT (kcal/mol)	−0.74	−0.73	−0.81	−1.06

[a]Each of two O lone pairs reported separately.

the electron donor N/P/O atom, with the observation that this decrease is smallest for the halogen bond in the last column. The next two rows pertain to orbital energies. There is some inconsistency in the lone pair energy in that even similar interactions such as P · · · N and P · · · P obey opposite trends. The energy of the pertinent P–H/C–Br σ^* antibonding orbital, however, is more uniform in that all rise, as might be anticipated for an interaction with an orbital of lower energy such as the occupied lone pair. It might be noted that this rise is quite a bit larger for the H-bond than for the P · · · N and halogen bonds.

A number of different measures have been discussed here of the energetic consequence of the transfer of electron density from one molecule to its partner. Three of these metrics are displayed in the last three rows of Table VII for purposes of comparison. The sum of one or more of the NBO second-order perturbation energies $E(2)$, that correspond to transfer from the lone pair to the σ^* orbital, lie between 1 and 3 kcal/mol. The smallest of these corresponds to the halogen bond, with the H-bond having the largest. The SAPT IND energy includes all contributions to the induction energy of the dimer, not just lp → σ^*. While this quantity is remarkably similar to $\sum E(2)$ for the two P · · · N/P bonds, the two measures are very different for the H and halogen bonds. The SAPT IND indicates the largest induction for the halogen bond, and smallest for the H-bond, precisely the opposite of the pattern in $\sum E(2)$. Turning to the KM CT energy in the last row, the quantities are fairly similar in magnitude, with the halogen bond term being the largest. It is concluded that no single measure of the energetics of charge transfer can be taken as the sole arbiter of this phenomenon.

Just as the NBO charge transfer parameters are associated with specific pairs of orbitals, and the charge transfer and induction energies refer to a sum over all such pairs, the same is true for the spatial aspects of charge transfer. For example, the NBO analysis of the P · · · N bond points toward a sizable transfer of density from the N lone pair to the σ^* antibonding orbital of a P–H bond. In apparent contrast, however, the density shift illustrated in Fig. 3(a) indicates that the lone pair of the N gains, rather than loses, density from the interaction. These two observations are not necessarily in contradiction, however, because the gain in the density of the N lone pair can arise from shifts from other parts of the NH_3 molecule or from PH_3, which occur in tandem with the particular lone pair → σ^* interorbital shift. Indeed, the same seeming paradox has been understood and accepted for years in the case of H-bonds, where a density shift from the lone pair orbital of the proton-accepting atom to the σ^* antibond of the bridging proton is contrasted with a gain in the total density in the lone pair region.

IV. SUMMARY AND DISCUSSION

The calculations outlined above have fleshed out some of the details of what appears to be a new sort of molecular interaction characterized by a weak noncovalent bond between P and N atoms. Unlike a H-bond, the P · · · N interaction requires no intermediacy of a H or other atom between P and N, relying on a direct attractive force between them. The attraction occurs when one P–H bond of PH_3 is oriented in such a way that its σ^* antibond overlaps with the lone pair of NH_3, so that electron density may be transferred from the latter to the former. Since the density is shifted into the lobe of the P–H σ^* that is proximate to the P atom, the process is facilitated by a nearly 180° disposition of the P–H to the N atom. This transfer is accompanied by an elongation of the pertinent P–H bond, weakened by additional density in its antibonding orbital. There is an analogous transfer from the P lone pair to an N–H σ^* antibond, although of lesser magnitude. The PH_3 homodimer adopts a very similar geometry, and is almost as strongly bound. Whereas the bridging H atom in a H-bond acquires a larger positive charge as a result of the bond, the H atom of the P–H covalent bond involved in the P · · · N interaction behaves in the opposite way, becoming more negatively charged.

Decomposition of the interaction energy suggests that the largest component of this P · · · N molecular interaction is electrostatic, followed by dispersion, and then by polarization + charge transfer. The trend is similar in the PH_3 homodimer, except that the electrostatic contribution diminishes, and dispersion grows accordingly with the replacement of the first-row N by P, making these two components similar in magnitude. Graphical display of the density shifts that accompany the dimer formation shows that, as is the case in H-bonds, a region of density increase is visible in the vicinity of the N lone pair, but other shifts are different from H-bonds. Rather

than the decrease around the bridging H observed in H-bonds, this loss occurs instead on the side of the P atom opposite the H atom. The buildup of charge seen in the bridging covalent X–H bond of a H-bond occurs instead on the H atom that is directly opposite the N.

The P···N bond also has certain features in common with halogen bonds, along with some fundamental differences. Whereas halogen bonds rely for part of their attractive force on a σ-hole of positive electrostatic potential that is present on the halogen atom, there is no such region on the P or N atoms. Perhaps as a consequence of the confined nature of the σ-hole, the halogen bond is extraordinarily sensitive to intermolecular orientation, vanishing in favor of alternate attractive forces in the face of even relatively small misorientations. In the particular case of $CH_3Br\cdots OCH_2$, there is a certain degree of charge transfer from the O lone pair to the C–Br σ^* antibond, reminiscent of the $N_{lp} \rightarrow \sigma^*(PH)$ shift in the P···N bond, but the C–Br bond elongation is vanishingly small. Also, the drop in occupation number of the O lone pairs in the halogen bond is considerably smaller than in either the P···N, P···P, or H-bonds. With respect to regional shifts of total electron density, P···N and H-bonds both exhibit a broad area of total density loss near the P or Br electron acceptor atom. However, the gain evident in the N lone pair region of P···N is absent around the corresponding O atom of Br···O. Energy decomposition analyses suggest that the halogen bond relies to a greater extent upon dispersion and charge transfer than does P···N but is less dependent upon electrostatic attraction.

There is a secondary minimum on the PH_3/NH_3 heterodimer potential energy surface, which contains a classical PH···N H-bond. This structure is less stable than the global minimum and is unbound when counterpoise and zero-point vibrational energies are included. Unlike a complex that is held together largely by dispersion, the potential energy surface of the heterodimer is quite anisotropic. The transition between the two minima on the surface passes through a region that is scarcely bound, with a significant energy barrier separating these two minima. The second minimum on the surface of the PH_3 homodimer is anomalous, very weakly bound, and contains neither a classical H-bond nor a geometry that would be conducive to charge shifts, and indeed shows no shifts of any magnitude at all. It appears to be held together primarily by dispersion, with only a small electrostatic contribution.

The importance of dispersion, or other factors that might be ignored at the Hartree–Fock level, to these complexes is underscored by the fact that earlier searches of these surfaces that did not include electron correlation identified completely different geometries as minima. In the case of the PH_3 homodimer, for example, an earlier exploration of the Hartree–Fock surface[75] did not identify either of the minima observed here. A later study[76] of the mixed PH_3/NH_3 dimer, again without correlation, erroneously identified geometries with H-bonded structures as minima. These observations suggest that H-bonded geometries are favored by forces that occur at the uncorrelated level, e.g., electrostatics and charge transfer.

These results lead to a question about the nature of the peripheral atoms in the two subunits. In structures such as **1a** or **5a**, the H atoms are pointing away from the central bonding region of the complex. It is natural to wonder then how a replacement of these H atoms by others, e.g., F, might affect the nature and strength of this interaction. In addition to altering the nature of the pertinent σ^* antibonding orbitals, such changes would affect other aspects of the interaction such as electrostatics and induction energy. This issue will be addressed in future work.

ACKNOWLEDGMENTS

I am indebted to Dr. Tapas Kar for assistance with some of the computations.

[1] P. Hobza and R. Zahradnik, *Weak Intermolecular Interactions in Chemistry and Biology* (Elsevier, Amsterdam, 1980).
[2] I. G. Kaplan, *Theory of Molecular Interactions* (Elsevier, Amsterdam, 1986).
[3] P. Hobza and R. Zahradnik, *Intermolecular Complexes* (Elsevier, Amsterdam, 1988).
[4] K. Müller-Dethlefs and P. Hobza, Chem. Rev. **100**, 143 (2000).
[5] A. J. Stone, *The Theory of Intermolecular Forces* (Oxford University Press, Oxford, 2002).
[6] P. Hobza and K. Muller-Dethlefs, *Non-Covalent Interactions* (RSC, Cambridge, 2010).
[7] G. C. Pimentel and A. L. McClellan, *The Hydrogen Bond* (Freeman, San Francisco, 1960).
[8] *The Hydrogen Bond. Recent Developments in Theory and Experiments*, edited by P. Schuster, G. Zundel, and C. Sandorfy (North-Holland, Amsterdam, 1976).
[9] D. Hadzi and S. Bratos, in *The Hydrogen Bond. Recent Developments in Theory and Experiments*, edited by P. Schuster, G. Zundel, and C. Sandorfy (North-Holland, Amsterdam, 1976), vol. 2, p. 565.
[10] P. Schuster, *Hydrogen Bonds* (Springer-Verlag, Berlin, 1984).
[11] G. A. Jeffrey and W. Saenger, *Hydrogen Bonding in Biological Structures* (Springer-Verlag, Berlin, 1991).
[12] S. Scheiner, *Hydrogen Bonding. A Theoretical Perspective* (Oxford University Press, New York, 1997).
[13] G. R. Desiraju and T. Steiner, *The Weak Hydrogen Bond in Structural Chemistry and Biology* (Oxford University Press, New York, 1999).
[14] *Hydrogen Bonding—New Insights*, edited by S. J. Grabowski (Springer, Dordrecht, 2006).
[15] G. Gilli and P. Gilli, *The Nature of the Hydrogen Bond* (Oxford University Press, Oxford, UK, 2009).
[16] P. Hobza and C. Sandorfy, Can. J. Chem. **62**, 606 (1984).
[17] S. Cybulski and S. Scheiner, J. Am. Chem. Soc. **109**, 4199 (1987).
[18] P. Seiler, G. R. Weisman, E. D. Glendening, F. Weinhold, V. B. Johnson, and J. D. Dunitz, Angew. Chem., Int. Ed. Engl. **26**, 1175 (1987).
[19] Z. Latajka and S. Scheiner, J. Comput. Chem. **5**, 674 (1987).
[20] K. B. Wiberg, R. F. Waldron, G. Schulte, and M. Saunders, J. Am. Chem. Soc. **113**, 971 (1991).
[21] S. Scheiner, Y. Gu, and T. Kar, J. Mol. Struct.: THEOCHEM **500**, 441 (2000).
[22] P. D. Vaz, M. M. Nolasco, F. P. S. C. Gil, P. J. A. Ribeiro-Claro, and J. Tomkinson, Chem. Eur. J. **16**, 9010 (2010).
[23] B. J. v. d. Veken, S. N. Delanoye, B. Michielsen, and W. A. Herrebout, J. Mol. Struct. **976**, 97 (2010).
[24] V. I. Bakhmutov, *Dihydrogen Bond: Principles, Experiments, and Applications* (John Wiley and Sons, Hoboken, NJ, 2008).
[25] O. Takahashi, Y. Kohno, and M. Nishio, Chem. Rev. **110**, 6049 (2010).
[26] G. Orlova and S. Scheiner, J. Phys. Chem. A **102**, 4813 (1998).
[27] B. Michielsen, J. J. J. Dom, B. J. v. d. Veken, S. Hesse, Z. Xue, M. A. Suhm, and W. A. Herrebout, Phys. Chem. Chem. Phys. **12**, 14034 (2010).
[28] B. G. d. Oliveira and M. N. Ramos, Int. J. Quantum Chem. **110**, 307 (2009).
[29] I. Alkorta, J. Elguero, and J. E. D. Bene, Chem. Phys. Lett. **489**, 159 (2010).
[30] S. Rizzato, J. Bergès, S. A. Mason, A. Albinati, and J. Kozelka, Angew. Chem., Int. Ed. Engl. **49**, 7440 (2010).
[31] L. R. Falvello, Angew. Chem., Int. Ed. Engl. **49**, 10045 (2010).
[32] G. R. Desiraju, Angew. Chem., Int. Ed. Engl. **50**, 52 (2011).

[33]E. Arunan, G. R. Desiraju, R. A. Klein, J. Sadlej, S. Scheiner, I. Alkorta, D. C. Clary, R. H. Crabtree, J. J. Dannenberg, P. Hobza, H. G. Kjaergaard, A. C. Legon, B. Mennucci, and D. J. Nesbitt, "Defining the hydrogen bond: An account," Pure Appl. Chem. (in press).
[34]F. H. Allen, J. P. M. Lommerse, V. J. Hoy, J. A. K. Howard, and G. R. Desiraju, Acta Crystallogr. **B53**, 1006 (1997).
[35]P. L. Wash, S. Ma, U. Obst, and J. Rebek, J. Am. Chem. Soc. **121**, 7973 (1999).
[36]A. Karpfen, J. Phys. Chem. A **104**, 6871 (2000).
[37]T. Caronna, R. Liantonio, T. A. Logothetis, P. Metrangolo, T. Pilati, and G. Resnati, J. Am. Chem. Soc. **126**, 4500 (2004).
[38]P. Auffinger, F. A. Hays, E. Westhof, and P. S. Ho, Proc. Nat. Acad. Sci. U. S. A. **101**, 16789 (2004).
[39]P. Politzer, P. Lane, M. C. Concha, Y. Ma, and J. S. Murray, J. Mol. Model. **13**, 305 (2007).
[40]R. E. Rosenfield, R. Parthasarathy, and J. D. Dunitz, J. Am. Chem. Soc. **99**, 4860 (1977).
[41]F. T. Burling and B. M. Goldstein, J. Am. Chem. Soc. **114**, 2313 (1992).
[42]M. Iwaoka, S. Takemoto, and S. Tomoda, J. Am. Chem. Soc. **124**, 10613 (2002).
[43]F. R. Fischer, P. A. Wood, F. H. Allen, and F. Diederich, Proc. Nat. Acad. Sci. U. S. A. **105**, 17290 (2008).
[44]A. Choudhary, D. Gandla, G. R. Krow, and R. T. Raines, J. Am. Chem. Soc. **131**, 7244 (2009).
[45]M. V. Vener, A. N. Egorova, and V. G. Tsirelson, Chem. Phys. Lett. **500**, 272 (2010).
[46]W. Wang, J. Xin, Y. Zhang, W. Wang, and Y. Lu, Int. J. Quantum Chem. **111**, 644 (2011).
[47]M. Solimannejad, M. Gharabaghi, and S. Scheiner, J. Chem. Phys. **134**, 024312 (2011).
[48]M. J. Frisch, G. W. Trucks, H. B. Schlegel *et al.*, GAUSSIAN 03, Gaussian, Inc., Pittsburgh, PA, 2003.
[49]T. H. J. Dunning, J. Chem. Phys. **90**, 1007 (1989).
[50]S. F. Boys and F. Bernardi, Mol. Phys. **19**, 553 (1970).
[51]A. E. Reed, F. Weinhold, L. A. Curtiss, and D. J. Pochatko, J. Chem. Phys. **84**, 5687 (1986).
[52]A. E. Reed, L. A. Curtiss, and F. Weinhold, Chem. Rev. **88**, 899 (1988).
[53]M. W. Schmidt, K. K. Baldridge, J. A. Boatz, S. T. Elbert, M. S. Gordon, J. H. Jensen, S. Koseki, N. Matsunaga, and K. A. Nguyen, J. Comput. Chem. **14**, 1347 (1993).
[54]K. Kitaura and K. Morokuma, Int. J. Quantum Chem. **10**, 325 (1976).
[55]K. Morokuma and K. Kitaura, in *Chemical Applications of Atomic and Molecular Electrostatic Potentials*, edited by P. Politzer and D. G. Truhlar (Plenum, New York, 1981), p. 215.
[56]K. Szalewicz and B. Jeziorski, in *Molecular Interactions. From Van der Waals to Strongly Bound Complexes*, edited by S. Scheiner (Wiley, New York, 1997), p. 3.
[57]R. Moszynski, P. E. S. Wormer, B. Jeziorski, and A. Van Der Avoird, J. Chem. Phys. **103**, 8058 (1995).
[58]MOLPRO, a package of *ab initio* programs designed by H.-J. Werner and P. J. Knowles, version 2010, F. R. Manby, M. Schütz, P. Celani, *et al.*.
[59]G. Schaftenaar and J. H. Noordik, J. Comput.-Aided Mol. Des. **14**, 123 (2000).
[60]S. M. Cybulski and S. Scheiner, Chem. Phys. Lett. **166**, 57 (1990).
[61]A. C. Legon, Angew. Chem., Int. Ed. Engl. **38**, 2686 (1999).
[62]P. Metrangolo, H. Neukirch, T. Pilati, and G. Resnati, Acc. Chem. Res. **38**, 386 (2005).
[63]P. Politzer, J. S. Murray, and M. C. Concha, J. Mol. Model. **13**, 643 (2007).
[64]I. Alkorta, F. Blanco, M. Solimannejad, and J. Elguero, J. Phys. Chem. A **112**, 10856 (2008).
[65]J. P. M. Lommerse, A. J. Stone, R. Taylor, and F. H. Allen, J. Am. Chem. Soc. **118**, 3108 (1996).
[66]R. Glaser, N. Chen, H. Wu, N. Knotts, and M. Kaupp, J. Am. Chem. Soc. **126**, 4412 (2004).
[67]J.-W. Zou, Y.-J. Jiang, M. Guo, G.-X. Hu, B. Zhang, H.-C. Liu, and Q.-S. Yu, Chem. Eur. J. **11**, 740 (2005).
[68]O. K. Poleshchuk, V. Branchadell, B. Brycki, A. V. Fateev, and A. C. Legon, J. Mol. Struct.: THEOCHEM **760**, 175 (2006).
[69]K. A. Riley, J. S. Murray, P. Politzer, M. C. Concha, and P. Hobza, J. Chem. Theory Comput. **5**, 155 (2009).
[70]Z. P. Shields, J. S. Murray, and P. Politzer, Int. J. Quantum Chem. **110**, 2823 (2010).
[71]J. S. Murray, P. Lane, and P. Politzer, Int. J. Quantum Chem. **107**, 2286 (2007).
[72]M. I. Bernal-Uruchurtu, R. n. Hernandez-Lamoneda, and K. C. Janda, J. Phys. Chem. A **113**, 5496 (2009).
[73]M. Palusiak, J. Mol. Struct.: THEOCHEM **945**, 89 (2010).
[74]W. Zierkiewicz, D. Michalska, and T. Zeegers-Huyskens, Phys. Chem. Chem. Phys. **12**, 13681 (2010).
[75]M. J. Frisch, J. A. Pople, and J. E. Del Bene, J. Phys. Chem. **89**, 3664 (1985).
[76]J. E. Del Bene, J. Comput. Chem. **10**, 603 (1989).